Ethylene carbonate adsorption on the major surfaces of lithium manganese oxide $Li_{1-x}Mn_2O_4$ spinel ($0.000 < x < 0.375$): a DFT+*U*-D3 study

Brian Ramogayana,[1] David Santos-Carballal,[1, 2,3*] Pablo A. Aparicio,[2] Matthew G. Quesne,[2] Khomotso P. Maenetja,[1] Phuti E. Ngoepe,[1] and Nora H. de Leeuw[2, 3,4,†]

[1]*Materials Modelling Centre, School of Physical and Mineral Sciences, University of Limpopo, Private Bag x1106, Sovenga 0727, South Africa*

[2]*School of Chemistry, Cardiff University, Main Building, Park Place, Cardiff CF10 3AT, United Kingdom*

3Present address: School of Chemistry, University of Leeds, Leeds LS2 9JT, United Kingdom

[4]*Department of Earth Sciences, Utrecht University, Budapestlaan 4, 3584 CD Utrecht, The Netherlands*

Abstract

Understanding the surface reactivity of the commercial cathode material $LiMn_2O_4$ towards the electrolyte is important to improve the cycling performance of secondary lithium-ion batteries and to prevent manganese dissolution. In this work, we have employed spin-polarized density functional theory calculations with on-site Coulomb interactions and long-range dispersion corrections [DFT+*U*−D3−(BJ)] to investigate the adsorption of the electrolyte component ethylene carbonate (EC) onto the (001), (011) and (111) surfaces of the fully lithiated and partially delithiated $Li_{1-x}Mn_2O_4$ spinel ($0.000 < x < 0.375$). The surface interactions were investigated by evaluating the adsorption energies of the EC molecule and the surface free energies. Furthermore, we analyzed the impact of the EC adsorption on the Wulff crystal morphologies, the molecular vibrational frequencies and the adsorbate/surface charge transfers. The adsorption energies indicate that the EC molecule strongly adsorbs on the (111) facet, which is attributed to a bidentate binding configuration. We found that the EC adsorption enhances the stability of the (111) facet, as shown by the Wulff crystal morphologies. Although a negligible charge transfer was calculated between the spinel surfaces and the EC molecule, a large charge rearrangement takes place within the surfactant upon adsorption. The wavenumbers of the C=O stretching mode for the interacting EC molecule are red-shifted with respect to the isolated adsorbate, suggesting that this bond becomes weaker. The surface free energies show that both the fully lithiated and partially delithiated forms of the $LiMn_2O_4$ surfaces are stabilized by the EC molecule.

Keywords: Density functional theory, spinels, Li-ion batteries, surface chemistry

* D.Santos-Carballal@leeds.ac.uk

† N.H.deLeeuw@leeds.ac.uk

1. Introduction

Over the last few decades, renewable energy storage has become of significant interest in the development of electric vehicles, which could facilitate a lesser reliance on fossil fuels and thus lower impact on global warming. Although many studies have aimed at discovering or developing sustainable, earth-abundant and/or low-cost alternative materials [1, 2, 3], there is still no viable replacement for the current lithium-based batteries. However, the development of more efficient and stable cathode materials would offer a major step forwards in the performance of lithium-ion batteries. Various cathode materials have been studied, including $LiCoO_2$ [4, 5], $Li_3V_2(PO_4)_3$ [6], $LiMn_2O_4$ [7, 8], $Li_4Mn_5O_{12}$ [9], $LiFePO_4$ [10] and NMCs [11] in order to improve the electrochemical performance of lithium-ion batteries.

Among these materials, lithium manganese oxide ($LiMn_2O_4$) spinel has attracted the most attention as a potential cathode material because of its three-dimensional crystal structure that allows a reversible diffusion of Li^+ ions [12, 13]. Moreover, $LiMn_2O_4$ is considered a safer substitute for the currently commercialized $LiCoO_2$ owing to its low environmental impact, the abundance of manganese and its high energy density [14]. However, the use of $LiMn_2O_4$ spinel as a cathode material is limited by the irreversible facing of the capacity, which is attributed to the dissolution of manganese, electrolyte oxidation at high voltages, and the Jahn-Teller distortion of the octahedral Mn^{3+} atoms [15, 16].

A number of methods have attempted to mitigate the manganese dissolution, including (i) cation doping [17, 18]; (ii) the replacement of commercially used $LiPF_6$ as the electrolyte ionic conductor to limit the production of the scavenging hydrofluoric acid produced by its degradation [19, 20, 21]; and (iii) surface coating to create an artificial barrier that limits the direct electrode-electrolyte contact [22, 23, 24, 25]. However, there is currently no substitute ionic conductor for the electrolyte which has better conductivity, thermal stability and affordability than $LiPF_6$, whereas the alternative route of introducing dopant ions might change the spinel crystal structure, thereby affecting the Li^+ transport in the battery [26]. An effective electrolyte solvent will not only be a good solvent for the ionic conductor but will also improve the lifetime of $LiMn_2O_4$-based lithium-ion batteries. Guyomard et al. [27] demonstrated that alkyl carbonates, such as propylene carbonate (PC) [28], vinylene carbonate (VC) [29, 30], allyl ethyl carbonate (AEC) [31] and ethylene carbonate (EC), are some of the most stable solvents for the lithium-ion battery electrolytes. Numerous subsequent studies [32, 33, 34] have shown that the ethylene carbonate (EC) is the most stable electrolyte solvent and shows improved electrochemical performance. Compared to other commercially used electrolyte solvents,

EC has the largest dielectric constant ($\varepsilon \approx 90.5$) [35, 36] and melting point owing to its high molecular symmetry. However, the reactivity of EC at the spinel surface and its effect on the crystal morphologies is not yet completely understood.

In this work, we report on calculations based on the density functional theory to study the interaction between EC and the non-polar surfaces of the fully lithiated and partially delithiated spinel $Li_{1-x}Mn_2O_4$ material ($0.000 < x < 0.375$). We discuss the binding energies of EC on the (001), (011) and (111) surfaces, the nanoparticle morphologies for $Li_{1-x}Mn_2O_4$ before and after adsorption, the inter- and intra-phase charge transfers, and the molecular vibrational frequencies.

2. Computational methods

2.1 Calculation details

The surface spinel calculations were performed using spin-polarized density functional theory (DFT) techniques as implemented in the Vienna Ab initio Simulation Package (VASP) [37]. All calculations were carried out within the generalized gradient approximation (GGA) using the Perdew, Burke, and Ernzerhof (PBE) exchange-correlation functional [38]. The kinetic energy cut-off was fixed at 560 eV for the expansion of the Kohn-Sham (KS) valence states. A Γ-centred Monkhorst-Pack grid of 5x5x1 k-points was used for the integration in the reciprocal space of all surfaces. The core electrons and their interaction with the valence electrons were described using the projector augmented-wave (PAW) method [39] in the implementation of Kresse and Joubert [40]. The core electrons are comprised of the levels up to the 3*s* for manganese and 1*s* for carbon and oxygen, while all the electrons are treated as valence electrons for lithium and hydrogen. The semi-empirical method of Grimme with the Becke-Johnson damping [D3-(BJ)] [41, 42] was also included in our calculations to model the long-range dispersion interactions, which are required to describe the surfaces properly [43, 44, 45, 46, 47, 48]. Gaussian smearing with a width of 0.05 eV was set to improve the convergence of the Brillioun zone integrations during geometry optimizations [42]. The tetrahedron method with Blöchl corrections was used to obtain accurate electronic and magnetic properties as well as total energies [49]. The Hubbard correction [50] in the formulation of Dudarev et al. [51] was applied to improve the description of the localized 3*d* Mn electrons. We have used the effective parameter $U_{eff} = 4.0$ eV, which we developed in our study of the bulk properties of the fully lithiated $LiMn_2O_4$ [52] and which is within the range of values reported in the literature [53, 54, 55, 56].

The spinel $LiMn_2O_4$ has a face-centered cubic crystal structure with a space group $Fd\bar{3}m$ (No. 227) [57] and a lattice constant of a = 8.24 Å [58, 59]. In our calculations, we have ignored the changes in the crystal lattice, resulting from the introduction of Li vacancies, when modelling the delithiated phases. Indeed, only minor changes in the lattice parameter of the cathode material are expected since a major change in the structure of the cathode would mean loss of possible recharge ability leading to deterioration of the battery efficiency. Similar methodologies have been employed in previous studies [60, 61, 55]. Furthermore, we have run benchmarking calculations to establish the difference in lattice parameters and surface areas of the fully lithiated and partially delithiated surface. We found that the slabs showed minor changes with a difference of only ~0.02 Å, which is equivalent to 5% (see electronic supporting information). The structure consists of a cubic close-packed array of oxygen atoms occupying the 32*e* sites, where lithium and manganese atoms occupy one-eighth of the tetrahedral (8*a*) sites and one-half of the octahedral (16*d*) sites, respectively, [62] (see Figure 1a).

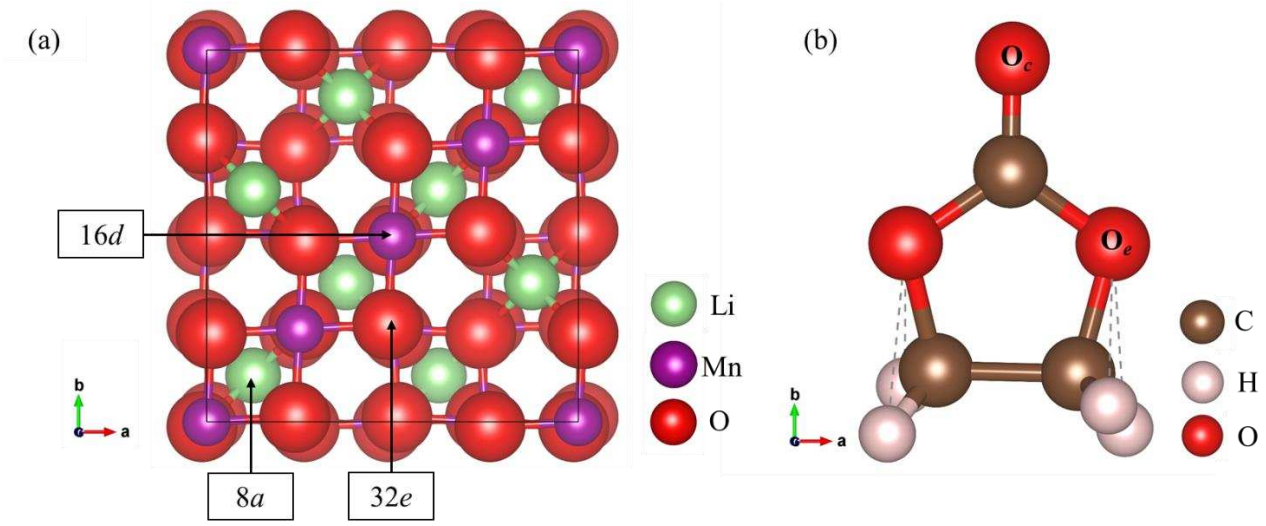

Figure 1: Schematic diagram of (a) conventional unit cell of $LiMn_2O_4$ spinel and (b) ethylene carbonate (EC) molecule, showing the ethereal (O_e) and carbonyl (O_c) oxygens.

2.2 Surface models

All the surface terminations were generated by cutting the geometry-optimized bulk structure [52], using the Tasker [63] dipole method, as implemented in METADISE (Minimum Energy Techniques Applied to Dislocations, Interfaces and Surface Energies) code [64], to create non-dipolar surfaces. The surfaces were represented by keeping fixed the atoms in the bottom-most layers at their relaxed bulk positions to simulate the bulk phase of $LiMn_2O_4$ and relaxing the rest the atoms during geometry optimization, resulting in a single relaxed slab. The surface areas, total number of layers and the

number of lithium atoms in the simulation cells considered for the fully lithiated and partially delithiated low-Miller index surfaces are shown in Table 1. The number of Li atoms with dangling bonds removed from the exposed layers of the fully lithiated $LiMn_2O_4$ are denoted by *x*. In every slab, a vacuum region of 15 Å was added perpendicularly to the surface to avoid interactions between the periodic images. We performed convergence tests with respect to the total number of layers, the number of relaxed atomic layers, and the vacuum thickness until the energy was constant within 1 meV of accuracy. We also applied dipole corrections perpendicular to the surface plane during our calculations, to enhance the convergence of the electronic energy. Geometry optimizations were conducted using the conjugate-gradient technique and were considered converged when the Hellmann-Feynman forces were below 0.01 eV/Å.

Table 1. Surface area ($A_{surface}$) and number of layers (N_{layers}) for each cell composition of the fully lithiated and partially delithiated surfaces of $Li_{1-x}Mn_2O_4$.

Surface	$A_{surface}$ $(Å^2)$	N_{layers}	Cell composition		*x*	
			Lithiated	Delithiated	Lithiated	Delithiated
(001)	69.72	9	$Li_8Mn_{16}O_{32}$	$Li_5Mn_{16}O_{32}$	0	0.375
(011)	49.30	9	$Li_8Mn_{16}O_{32}$	$Li_5Mn_{16}O_{32}$	0	0.375
(111)	60.38	13	$Li_8Mn_{16}O_{32}$	$Li_6Mn_{16}O_{32}$	0	0.250

For each surface orientation, we have modeled the two possible terminations using stoichiometric, non-polar and symmetric slabs along the *z*-direction, as shown in Figure 2. When constructing the surface terminations, we considered the stacking sequence for low Miller index facets [65, 66, 67, 68]. The (001) surface terminations were cleaved from atomic planes perpendicular to the [001] direction and consist of an alternation of Li and Mn/O planes. The top species in the (001) surface were 0.5 ML of Li atoms on the bulk-like Mn−O layer for termination *A* and two Mn for every four O atoms for termination *B*. The (111) facets were created from atomic planes consisting of six possible bulk-like surface terminations (O_1, Mn_1, O_2, Li_1, Mn_2 and Li_2) which are dipolar. However, upon reconstruction, only two non-dipolar terminations were possible for the (111), i.e. a Li- and a Li/Mn/O-termination. The (011) surface can be cleaved along the Li/Mn/O and Mn/O planes. The slabs were terminated by half of the Li/Mn/O and Mn/O bulk layers, respectively.

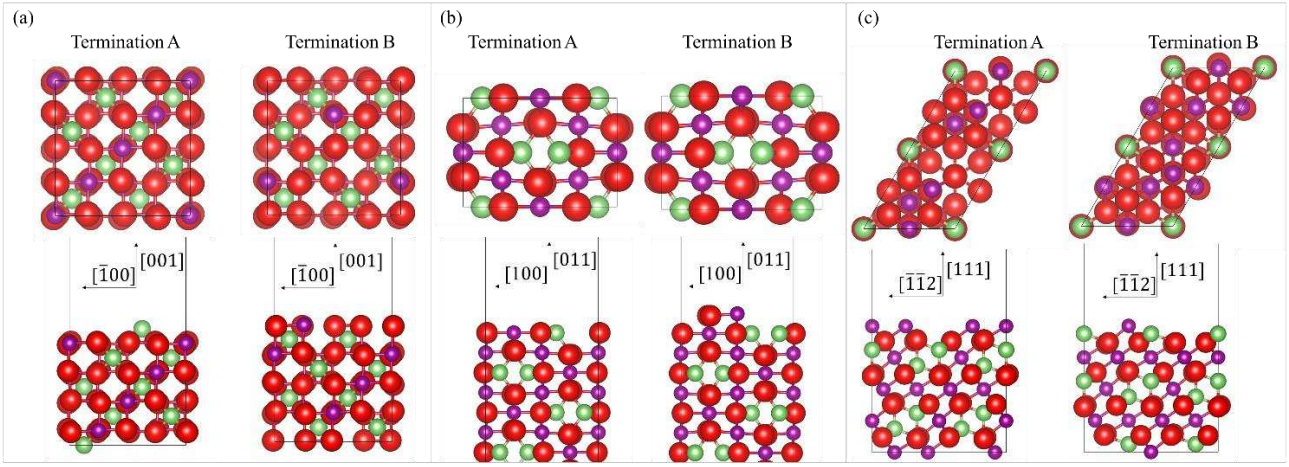

Figure 2: Top and side view of the simulated slabs for the fully lithiated $LiMn_2O_4$ spinel. Crystallographic directions for the top view of (001) surface terminations is [100] for the abscissae towards the right, for the (011) surface terminations it is $[0\bar{1}1]$ for the abscissae towards the right, and for the (111) surface terminations it is $[0\bar{1}1]$ for the longest axis towards the top.

2.3.Surface and adsorption energies

The surface energies were calculated for the relaxed and unrelaxed slabs. The unrelaxed surface energies (γ_u) were evaluated from static calculations as

$$\gamma_{\mathrm{u}} = \frac{E_{\mathrm{u,slab}} - E_{\mathrm{bulk}}}{2A} \quad (1)$$

where $E_{\mathrm{u,slab}}$ is the total energy of the unrelaxed slab, E_{bulk} is the total energy of the bulk with the same number of formula units as the slab and A is the surface area of the slab. The relaxed surface energies (γ_{r}) were also calculated for the spinel material following geometry optimization of the slab, where the bottom half of the layers were kept fixed at their relaxed bulk positions, while the top layers were allowed to relax. Since the slabs were comprised of both relaxed and unrelaxed sides, the relaxed surface energies were calculated as:

$$\gamma_{\mathrm{u}} + \gamma_{\mathrm{r}} = \frac{E_{\mathrm{r}},\mathrm{slab} - E_{\mathrm{bulk}}}{A} \quad (2)$$

where E_{r} is the total energy of the half-relaxed surface. The degree of relaxation (R) was also calculated for all the surfaces as:

$$R = \frac{\gamma_{\mathrm{u}} - \gamma_{\mathrm{r}}}{\gamma_{\mathrm{u}}} \times 100 \quad (3)$$

To characterize the interaction of EC on both the fully lithiated and partially delithiated (001), (011) and (111) spinel facets, we have calculated the adsorption energy (E_{ads}) for different adsorption sites at different orientations of the molecule. The adsorption energy was calculated according to the equation:

$$E_{\mathrm{ads}} = E_{\mathrm{EC+slab}} - (E_{\mathrm{EC}} + E_{\mathrm{slab}}) \quad (4)$$

where $E_{\mathrm{EC+slab}}$ is the total energy of the slab with the EC molecule adsorbed, E_{EC} is the total energy of the isolated EC molecule and E_{slab} is the total energy of the pristine slab. The energy minimization for an isolated EC molecule was performed sampling only the Γ point of the Brillouin zone using a cell of $10\ \text{Å} \times 11\ \text{Å} \times 12\ \text{Å}$ to avoid spurious interactions. A positive value of E_{ads} indicates an endothermic and unfavourable adsorption process, whereas a negative value indicates an exothermic and favourable adsorption process.

We further calculated the surface free energies (σ) for the modified slabs, *i.e.* when it is partially delithiated or interacting with the EC molecule via the equation:

$$\sigma = \gamma_{\mathrm{r}} + \frac{E_M - E\mathrm{r} + (8 - N_{\mathrm{Li}})E_{\mathrm{Li}} - E_{\mathrm{EC}}}{A} \quad (5)$$

where E_{M} is the energy of the modified slab, $8-N_{\mathrm{Li}}$ is the number of lithium atoms removed from the slab, E_{Li} is the energy of one atom in the bulk of the body-centred cubic (*bcc*) lithium, E_{r} is the energy of the pristine slab and E_{EC} is the energy of the isolated ethylene carbonate molecule. Where there is no surface modification, the surface energies and the surface free energies have the same value, but a correction expression is added to account for surface modifications, such as adsorptions, doping, delithiation and lithiation.

2.4. Vibrational frequencies

Vibrational frequencies for the isolated and adsorbed EC molecule were calculated using the central finite differences approach. The method comprises calculations of vibrational frequencies from the second derivatives of the potential energy with respect to the atomic positions. These were allowed to move by small displacements in the three Cartesian planes to ensure they fall within the harmonic part of the potential well. The fundamental vibrational modes were classified into symmetric (υ_{sym}) and asymmetric stretching (υ_{asy}), as well as bending (δ) modes.

2. Results and discussions

3.1. Surface energies

The stabilities of the surface terminations obtained from the fully optimized spinel bulk structure [52] were analyzed by calculating the surface energies for the unrelaxed and relaxed slabs, see Table 2. Before and after relaxation, we observed the same trend of increasing surface energies and decreasing stability, which is (001) < (011) < (111). We also observed that termination *A* of the (001) surface, i.e. the Li-terminated $LiMn_2O_4$ surface, is the most stable plane with $\gamma_r = 0.04$ eV/Å^2. This lowest energy termination is in agreement with the reported literature [56, 55], and also compares well with the lowest energy of the Mg-terminated $MgAl_2O_4$ surface [69]. Among all the surface terminations, the (111) termination *B* showed the largest geometry relaxation. For the sake of simplicity and to identify the salient behaviour of the surfaces interacting with the ethylene carbonate, we have as an approximation neglected in this study potentially modifying factors such as an external field caused by the double layer generated on the surface, voltage or electric current.

Table 2. Calculated surface energies for the unrelaxed (γ_u) and relaxed (γ_r) slabs of the low-Miller index surfaces of the fully lithiated $LiMn_2O_4$.

Surfaces	Termination	γ_u (eV/Å^2)	γ_r (eV/Å^2)	Relaxation (%)
(001)	*A*	0.07	0.04	43.7
	B	0.15	0.11	28.7
(011)	*A*	0.10	0.05	50.0
	B	0.10	0.07	37.2
(111)	*A*	0.08	0.05	38.0
	B	0.21	0.09	57.9

3.2. Ethylene carbonate adsorption

Here, we discuss the spinel surface interactions towards the ethylene carbonate electrolyte component. First, we explored the preferred adsorption geometries for different orientations of the EC molecule and various binding sites on the $Li_{1-x}Mn_2O_4$ (001), (011) and (111) surfaces. The adsorption sites investigated included the atop, bottom, bridge, and hollow positions, as shown in Figure 3. The initial interaction configurations of the EC molecule included coordination to the surface via the carbonyl and ethereal oxygen, both in flat and perpendicular orientations. Before

adsorption, we measured the structural parameters of the relaxed EC molecule and compared them with the available literature data to ensure the accuracy of our results. Table 3 summarises the equilibrium bond distances and angles, and which are in good agreement with the available literature.

Table 3. The equilibrium bond distances and angles in the EC molecule calculated and compared to literature.

Parameters	This work	Experimental [70]	B3PW91 [71]	Monte Carlo [72]
d(C=O)/Å	1.20	1.20	1.15	1.20
d(C-O)/Å	1.37	1.39	1.33	1.36
d(C-C) /Å	1.50	1.54	1.52	1.43
d(C-H) /Å	1.10	1.09	-	1.09
∠(O-C-O) /°	110.5	125.2	124.1	110.6
∠(C-O-C) /°	108.9	109.5	109.0	110.5

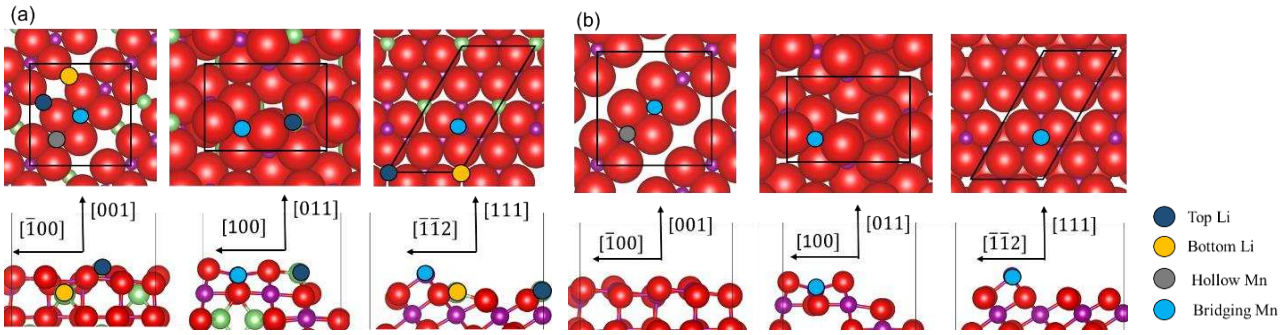

Figure 3. Top and side view of the modelled slabs for (a) the fully lithiated $LiMn_2O_4$ and (b) the partially delithiated $Li_{1-x}Mn_2O_4$. Crystallographic directions for the top view of (001) surface terminations is [100] for the abscissae towards the right, for the (011) surface terminations it is [0$\bar{1}$1] for the abscissae towards the right, and for the (111) surface terminations it is [0$\bar{1}$1] for the longest axis towards the top.

In all our simulations, the EC molecule was placed initially at 2.5 Å from the surface to favour the attractive forces over the repulsive ones between the molecule and the surface. However, during geometry optimization, the adsorbate and the surface were free to move and allowed to change their adsorption geometry. Figure 4 displays the most stable interactions between the EC molecule and the $Li_{1-x}Mn_2O_4$ surfaces, together with the relevant binding energies. First, we explored the EC

adsorption onto the fully lithiated spinel surface through the Mn atom, where our calculations indicate that the EC molecule prefers to bind to the surface through the carbonyl oxygen at a distance of 2.47 Å, when placed parallel to the surface. This mode is in excellent agreement with previous work [73], where the EC molecule was found to bind strongly to the fully lithiated spinel (001) surface through the Mn atom. In our work, we also explored the EC adsorption on the (001), (011) and (111) where we found that the process releases the largest adsorption energy at the (111) facets due to bidentate binding modes to the Li and Mn atoms. Next, we studied the EC adsorption onto the fully lithiated surfaces through the Li atom, where it strongly binds with the surfaces through the ethereal oxygen (O_e). However, upon geometry optimization, the molecule interacted with the exposed Mn and Li atoms in (111) surface with a very exothermic adsorption energy. The EC molecule preferred to interact with the (001) Li atom through the ethereal oxygen at a distance of 2.31 Å and by forming one hydrogen-bond of 2.16 Å with one surface oxygen. Moreover, the EC molecule was found to bind perpendicularly to the (011) surface at 2.00 Å via the ethereal oxygen. We also studied the EC adsorption onto the partially delithiated surfaces, where the only available adsorption sites are the exposed manganese atoms. Similar to the (001) lithiated surfaces, the EC molecule preferred to bind with the delithiated surfaces through the carbonyl oxygen where the strongest binding energy was calculated on the (111) facet.

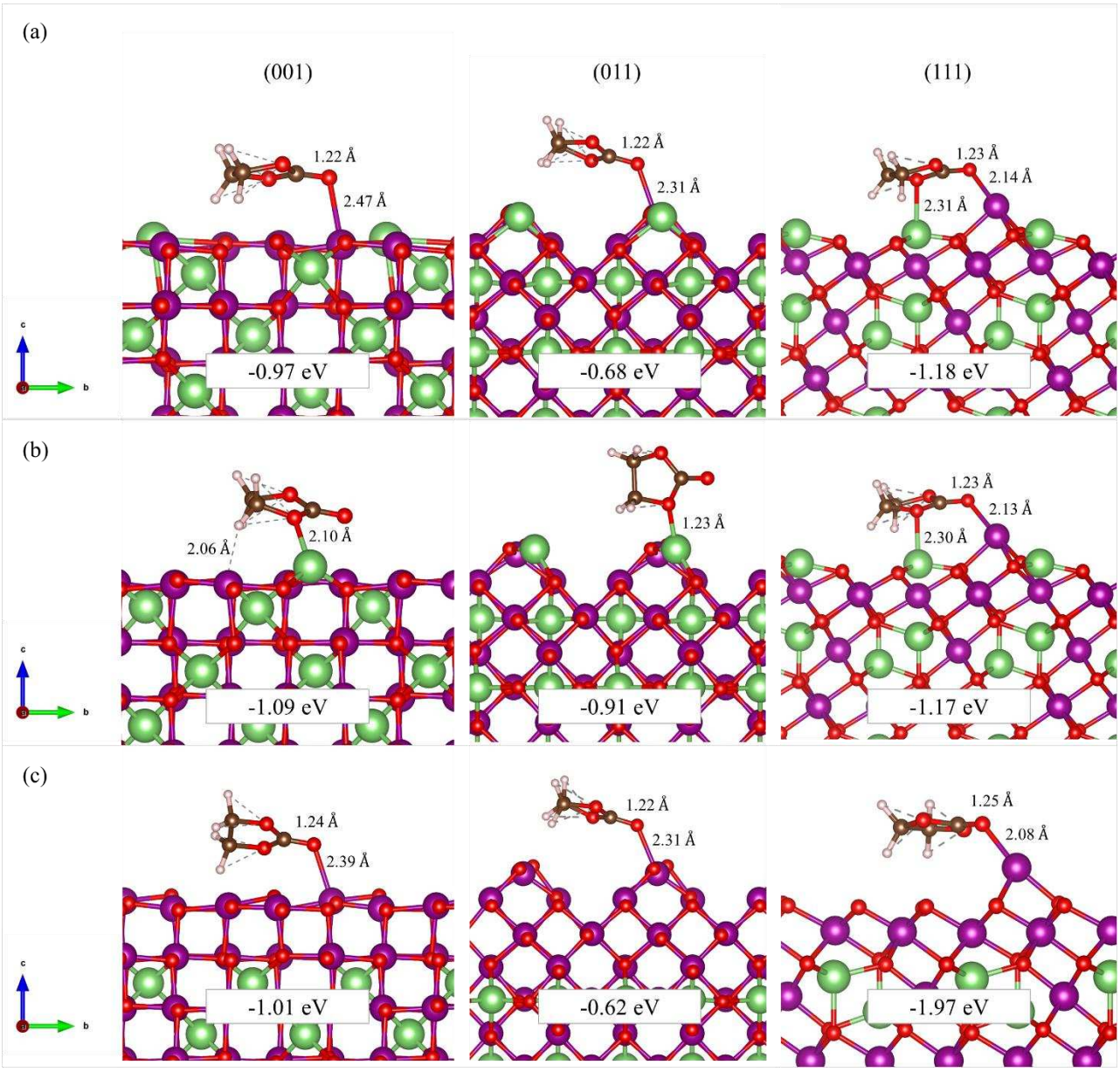

Figure 4. Most stable adsorption configurations for the EC molecule on the $Li_{1-x}Mn_2O_4$ surfaces. Adsorption sites in the fully lithiated spinel are (a) Mn atom, (b) Li atom; and in the partially delithiated surface it is (c) Mn atom. Crystallographic directions for the top view of (001) surface terminations is [100] for the abscissae towards the right, for the (011) surface terminations it is $[0\bar{1}1]$ for the abscissae towards the right, and for the (111) surface terminations it is $[0\bar{1}1]$ for the longest axis towards the top.

252 3.3.Surface free energies

253 Table 4 summarises the surface free energies of the fully lithiated surfaces interacting with the EC
254 molecule, as well as the partially delithiated surfaces, both pristine and interacting with the adsorbate.
255 The calculated surface free energies are higher as compared to the surface energies of the fully-
256 lithiated facets. This increase in energy of the partly delithiated surfaces as compared to the fully
257 lithiated surfaces indicates that upon delithiation, the surfaces become less stable, thus a destabilising
258 effect. However, the addition of the EC molecule can affect the stabilities of both the fully lithiated
259 and partially delithiated systems. For example, when the EC molecule is adsorbed onto the (001)
260 surface by coordinating one of the manganese atoms, an increase of 0.08 eV/Å^2 in the surface free
261 energy is observed, indicating that the adsorbate has a destabilizing effect. On the other hand, we
262 have also observed a decrease in the surface free energies for the other modified surfaces with respect
263 to the pristine planes, but proportionally smaller than in the (011) facet [44].

264 Table 4: Surface free energy (σ) for the fully lithiated and partially delithiated $Li_{1-x}Mn_2O_4$ surfaces
265 interacting with the EC molecule.

Surface	x	Adsorption site	$\boldsymbol{\sigma}$ (eV/Å^2)
(001)	0	Mn	0.12
	0	Li	0.02
	0.375	–	0.13
	0.375	Mn	0.02
(011)	0	Mn	0.13
	0	Li	0.04
	0.375	–	0.13
	0.375	Mn	0.04
(111)	0	Mn	0.07
	0	Li	0.02
	0.250	–	0.11
	0.250	Mn	0.02

266

267 3.4. Morphology

268 Here we discuss the Wulff crystal morphologies for the fully lithiated and partially delithiated
269 $Li_{1-x}Mn_2O_4$, which were obtained using the termination with the lowest surface free energy for each
270 pristine and modified surface [74, 75]. As shown in Figure 5, the (001) plane dominates the
271 morphologies for the fully lithiated material and the (111) is the major surface for the partially
272 delithiated spinel. The (011) surface does not appear in the Wulff morphology after delithiation or

adsorption of the EC molecule, because of its higher surface free energy with respect to the (001) and (111) planes. We have also carried out test calculations to determine the effect of different Li content and found similar Wulff crystal morphologies to the ones represented in figure 5 using slabs containing the same stoichiometry (see electronic supporting information). Our morphology for the delithiated material interacting with the electrolyte is in excellent agreement with the work of Kim et al. [76], who found that the octahedron-shaped $Li_{1-x}Mn_2O_4$ particles are dominated by the (111) surface.

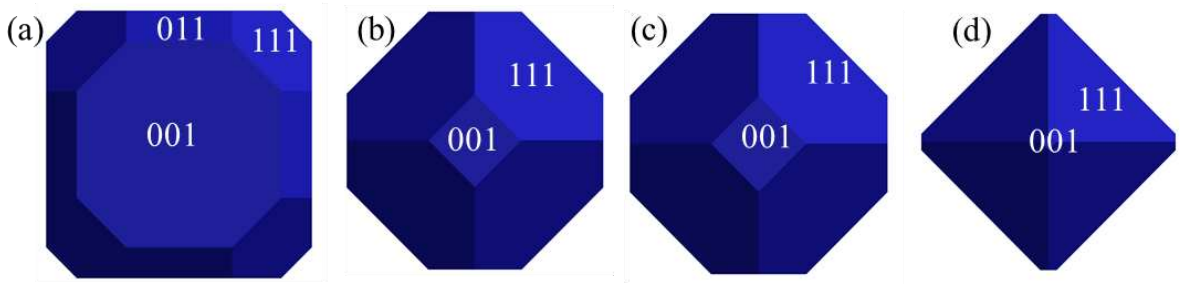

Figure 5. Surface morphologies for $Li_{1-x}Mn_2O_4$, (a) before and (b) after adsorption of EC on the fully lithiated spinel, (c) before and (d) after adsorption of EC on the partially delithiated material.

3.5. Charge transfer and work function

We have carried out a Bader charge analysis to quantify the electron transfer upon adsorption of the electrolyte to the surfaces of the cathode (Table 5). For all the adsorbed systems, we generally observe a negligible charge transfer which suggests that this process only plays a minor role in the adsorption mechanism. The largest charge transfer of Δq = -0.05 e^- was observed at the Li site of the (001) surface. We further explored the electronic structure by plotting the charge density difference for the adsorption configuration with the largest inter-phase charge transfer, see Figure 6. Despite the surface donating a minor charge to the electrolyte molecule, the electron flow is dominated by an internal charge rearrangement within the EC molecule. We have also compared the charge transfer between the carbonyl oxygen (O_c) and the directly bonded atoms following adsorption, by subtracting from the charge density of the total adsorbate-surface system the sum of the charge density of the isolated adsorbate and clean surface in the same geometry. We observe partial oxidation of carbon and reduction of oxygen, owing to intramolecular electron rearrangement caused by the electron transfer from the C=O π-bond to an oxygen-surface σ-bond. In all cases, there is transfer of ~1 electron from the carbon to the oxygen, which could lead to heterolytic cleavage of the C=O π-bond under working conditions. We have also compared the charge difference between the O_e in the isolated and adsorbed

molecule, when it is interacting with the surface via this atom. We generally observe a minor charge acumulation on the O_e, which suggests that the ethereal bond is unlikely to break upon adsorption of the EC molecule to the surface.

We next calculated the work function (Φ) for the modified surfaces, which measures the energy required to bring a surface electron to the vacuum [46]. Generally, we observe a decrease in the work function as we adsorbed the molecule, although in the delithiated surfaces the work function remains fairly constant. The lowest value of the work function is observed when the EC molecule is adsorbed on the pristine surfaces through the lithium (Li-O).

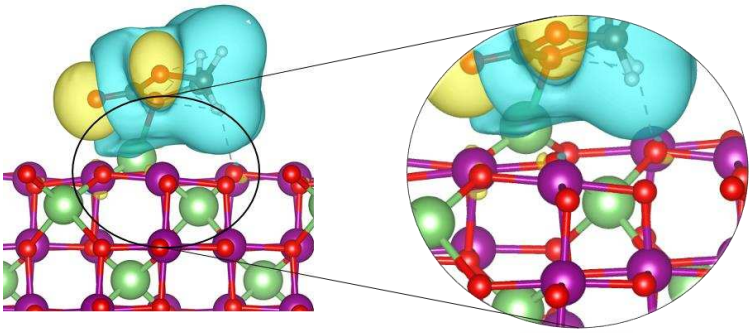

Figure 6. Charge density flow ($\Delta\rho$) for the EC molecule adsorbed on the $LiMn_2O_4$ (001) surface. The charge density difference schemes were constructed by subtracting the sum of the electron charge densities of the clean surface and isolated adsorbate, with identical structures as in the adsorbed form, from the electron density of the total adsorbate-surface system. The electron density gain and depletion are represented by yellow and blue respectively. The isosurfaces display a value of 0.003 e $Å^{-3}$; the purple spheres indicate the manganese atoms, red spheres indicate the oxygen atoms and the green spheres represent the Li atoms.

Table 5: Charge transfer between the surface and EC molecule (Δq_{EC}) as well as the charge accumulation/depletion on the carbonyl and ethereal oxygen ($\Delta q_{\mathrm{Oc/Oe}}$), and work function for the surfaces before (Φ_p) and after (Φa) adsorption. The vibrational wavenumbers are also included to describe the symmetric stretching (ν_{sym}), asymmetric stretching (ν_{asym}) and bending (δ) modes.

							CH_2 vibrations			C=O
Surface	Adsorption site	x	Δq_{EC} (e^-)	$\Delta q_{\mathrm{Oc/Oe}}$ (e^-)	Φ_p (eV)	Φ_a (eV)	υ_{sym} (cm^{-1})	υ_{asy} (cm^{-1})	δ (cm^{-1})	υ (cm^{-1})
Isolated EC				0.00			2952	2990	1341	1829
EC (liquid films) [77]							2928	2955	1397	1803
(001)	Mn	0	-0.02	0.81 (O_c)	4.53	3.45	2994	2917	1489	1733
	Li	0	-0.05	0.07 (O_e)	4.53	3.16	2968	3043	1456	1770
	Mn	0.375	0.02	0.83 (O_c)	3.34	3.56	3028	3079	1465	1747
(011)	Mn	0	0.00	0.80 (O_c)	4.74	4.45	3021	3048	1477	1740
	Li	0	-0.01	0.03 (O_e)	4.74	4.26	3024	3089	1479	1787
	Mn	0.375	0.02	0.81 (O_c)	3.82	3.82	2998	3084	1479	1736
(111)	Li, Mn	0	0.00	0.78 (O_c)	3.66	3.55	2978	3007	1476	1705
	Li, Mn	0	0.02	0.08 (O_e)	3.66	3.57	3012	3065	1473	1720
	Mn	0.250	0.04	0.78 (O_c)	3.62	3.62	3001	3034	1443	1659

3.6. Vibrational frequencies

In order to characterize further the EC surface adsorption, we have computed the wavenumbers of the fundamental vibrational modes for the lowest-energy adsorption geometries on the (001), (011) and (111) spinel surfaces (Table 5). The quality of the vibrational modes calculated for the isolated EC molecule was assessed by comparing them with the experimental values. Our simulated vibrational modes for the isolated EC molecule compare closely with the experimental data, with the largest difference being 56 cm^{-1}. For example, the asymmetric and symmetric υ(C-H) stretching modes for the free EC molecule were computed at 2952 and 2990 cm^{-1}, which compares well with the experimental values of 2928 and 2955 cm^{-1}, respectively. These hydrogen stretching modes are blue-shifted as a result of steric effects, since the hydrogen atoms are less mobile. We also analysed the C=O stretching modes for the adsorbed EC molecule, which were in the range of 1700 – 1900 cm^{-1} as reported by Fortunato et al [78]. Although we observed a minimal charge transfer between the molecule and the surface, this does not prevent the stretching of the C=O bond. Our simulations

indicate that the vibrational modes are red-shifted with respect to the isolated EC molecule, suggesting that the internal bonds in the adsorbate weaken upon adsorption onto the spinel surfaces. This phenomenon was also observed in the charge transfers, where the carbonyl oxygen gains electron density from the carbon atom, which further weakens the C=O bond.

Conclusions

DFT simulations have been performed to study the adsorption of the ethylene carbonate molecule on the fully lithiated and partially delithiated $Li_{1-x}Mn_2O_4$ spinel surfaces. The lithium-terminated (001) surface was found to be the most stable facet, which agrees with the reported literature. We further investigated the partially delithiated surfaces, where we observed a larger surface free energy with respect to the fully lithiated surface, indicating the destabilizing effect of delithiation.

We observed the strongest adsorption of the EC on the (111) surface, which was attributed to the EC molecule interacting with both the manganese and lithium atoms in the surface. The surface free energy was found to decrease following interaction with the adsorbate, which thus stabilizes the material. The Wulff morphologies show that EC adsorption enhances the expression of the (111) facet. Negligible charge transfer was observed between the adsorbate and surfaces, and the charge density flow shows a strong electronic rearrangement within the EC molecule. The electron density on the carbonyl oxygen is increased, due to partial carbon oxidation and oxygen reduction, i.e. an intramolecular electron rearrangement from the C=O π-bond to an oxygen-surface σ-bond. The vibrational frequencies also showed a red-shift in the C=O stretching mode of the adsorbed EC with respect to the isolated molecule, which suggests the weakening of the C=O bond. Our simulations show that the EC solvent binds to the spinel surfaces, releasing moderate adsorption energies. We speculate that this binding protects the surface against Mn dissolution, while still allowing the EC molecule to detach easily when the $LiPF_6$ ionic conductor approaches the surface to react with its Li atoms. Moreover, the lack of charge transfer between the surfaces and the EC molecule indicates that the solvent acts as a protective layer which shows no reactivity towards the spinel, but remains stable while adsorbed. Furthermore, the particle morphologies indicate that upon surface delithiation, the (111) facet becomes the most stable surface, which has also been reported as the surface that is most resistant to manganese dissolution. In future work, we aim to explore explicit solvation of the spinel surfaces during the charge/discharge processes, in addition to obtaining a clear understanding of the kinetics and thermodynamics of the EC decomposition on the surfaces

Acknowledgments

D.S.-C. is grateful to the Department of Science and Technology (DST) and the National Research Foundation (NRF) of South Africa for the provision of a Postdoctoral Fellowship for Early Career Researchers from the United Kingdom. P.E.N. acknowledges the financial support of the DST-NRF South African Research Chair Initiative. We also appreciate the support received from DST Energy Storage Research Development and Innovation Initiative. We acknowledge the Engineering & Physical Sciences Research Council (EPSRC Grant No. EP/K009567/2 and No. EP/K016288/1), the Economic and Social Research Council (ESRC Grant ES/N013867/1) and National Research Foundation, South Africa, for funding of a grant for UK-SA PhD exchanges under the Newton programme. This work was performed using the computational facilities of the Advanced Research Computing @ Cardiff (ARCCA) Division, Cardiff University; the Centre for High Performance Computing (CHPC) of South Africa; and the Supercomputing Facilities at Cardiff University operated by ARCCA on behalf of the HPC Wales and Supercomputing Wales (SCW) projects. We acknowledge the support of the latter, which is part-funded by the European Regional Development Fund (ERDF) via Welsh Government. All data created during this research is openly available from the Cardiff University's Research Portal at http://doi.org/10.17035/d.2019.0085116020

Conflicts of interest

There are no conflicts to declare.

Reference

[1] P.A. Aparicio, J.A. Dawson, M.S. Islam and N.H. De Leeuw, *J. Phys. Chem. C,* 2018, **122**, 25829 - 25836.

[2] L. Wang, Y. Lu, J. Liu, M. Xu, J. Cheng, D. Zhang, and J.B. Goodenough, *Angew. Chem. Int. Ed.,* 2013, **125**, 2018 - 2021.

[3] L. Xu, H. Li, X. Wu, M. Shao, S. Liu, B. Wang, G. Zhao, P. Sheng, X. Chen, Y. Han and Y. Cao, *Electrochem. Commun.,* 2019, **98,** 79 - 81.

[4] P. Byeon, H.B. Bae, H.S. Chung, S.G. Lee, J.G. Kim, H.J. Lee, J.W. Choi and S.Y. Chung, *Adv. Funct. Mater.,* 2018, **28**, 1804564.

[5] K. Ozawa, *Solid State Ionics,* 1994, **69**, 212 - 221.

[6] D.W. Han, S.J. Lim, Y.I Kim, S.H. Kang, Y.C. Lee and Y.M. Kang, *Chem. Mater.,* 2014, **26**, 3644 - 3650.

[7] W. Tang, Y. Hou, F. Wang, L. Liu, Y. Wu and K. Zhu, *Nano Lett.,* 2013, **13**, 2036 - 2040.

[8] C.Y. Ouyang, S.Q. Shi, Z.X. Wang, H. Li, X.J Huang and L.Q. Chen, *Europhys. Lett.,* 2004, **67**, 28.

[9] R.S. Ledwaba, M.G. Matshaba and P.E. Ngoepe, *IOP Conf. Ser., Mater. Sci. Eng.,* 2015, **80**, 012024.

[10] T. Mueller, G. Hautier, A. Jain and G. Ceder, *J. Mater. Chem.,* 2011, **23**, 3854 - 3862.

[11] D. Andre, S.J. Kim, P. Lamp, S.F. Lux, F. Maglia, O. Paschos and B. Stiaszny, *J. Mater. Chem. A,* 2015, **3**, 6709 - 6732.

[12] J. Kim and A. Marnthiram, *Nature,* 1997, **390**, 265 - 267.

[13] S.T. Lee, K. Raveendranath, R.M. Tomy, N.A. George, S. Jayalekshmi and J. Ravi, *J. Phys. D: Appl. Phys.,* 2007, **40**, 3807 - 3810.

[14] N. Bensalah and H. Dawood, *J. Mater. Sci. Eng.,* 2016, **5**, 1 - 21.

[15] Y.Y. Xia, T. Sakai, T. Fujieda, X.Q. Yang, X. Sun, Z.F. Ma, J. McBreen and M. Yoshio, *J. Electrochem. Soc,* 2001, **148**, A723 - A729.

[16] M. Wohlfahrt-Mehrens, C. Vogler and J. Garche, *J. Power Sources,* 2004, **127**, 58 – 64.

[17] M. Michalska, D.A. Ziółkowska, J.B. Jasiński, P.-H. Lee, P. Ławniczak, B. Andrzejewski, A. Ostrowski, W. Bednarski, S.H. Wu and J.Y. Lin, *Electrochim. Acta,* 2018, **276**, 37 - 46.

[18] A. M. Kannan and A. Manthiram, *Electrochem. Solid-State Lett.,* 2002, **5**, 167 - 169.

[19] S. Brox, S. Röser, T. Husch, S. Hildebrand, O. Fromm, M. Korth, M. Winter and I. Cekic-Laskovic, *ChemSusChem,* 2016, **9**, 1704 - 1711.

[20] H.Q. Gao, Z.A. Zhang, Y.Q. Lai, J. Li and Y.X. Liu, *J Cent South Univ T,* 2008, **15**, 830 - 834.

[21] S. Hwang, D.H. Kim, J.H. Shin, J.E. Jang, K.H. Ahn, C. Lee and H. Lee, *J. Phys. Chem.,* 2018, **122**, 19438 - 19446.

[22] D. Guan, J.A. Jeevarajan and Y. Wang, *Nanoscale,* 2011, **3**, 1465 - 1469.

[23] S. Hao and C. Wolverton, *J. Phys. Chem. C,* vol. 117, no. 16, pp. 8009 - 8013, 2013.

[24] S.C. Park, Y.M. Kim, Y.M. Kang, K.T. Kim, P.S. Lee and J.Y. Lee, *J. Power Sources,* 2001, **103**, 86 - 92.

[25] S. Lim and J. Cho, *Electrochem. Commun.,* 2008, **10**, 1478 - 1481.

[26] M. Aykol, S. Kirklin and C. Wolverton, *Adv. Energy Mater.,* 2014, **4**, 1400690.

[27] D. Guyomard and J.M. Tarascon, *J. Electrochem. Soc.,* 1992, **139**, 937 - 948.

[28] S.I. Tobishima and T. Okada, *Electrochim. Acta,* 1985, **30**, 1715 - 1722.

[29] Y. Hu, W. Kong, H. Li, X. Huang and L. Chen, *Electrochem. Commun.,* 2004, **6**, 126 - 131.

[30] M. Fujimoto, Y. Shouji, T. Nohma and K. Nishio, *Denki Kagaku,* 1997, **65**, 949 - 953.

[31] J.T. Lee, Y.W. Lin and Y.S. Jan, *J. Power Sources,* 2004, **132**, 244 - 248.

[32] L. Xing, W. Li, C. Wang, F. Gu, M. Xu, C. Tan and J. Yi, *J. Phys. Chem. B,* 2009, **113**, 16596 - 16602.

[33] J.C. Soetens, C. Millot and B. Maigret, *J. Phys. Chem. A,* 1998, **102**, 1055 - 1061.

[34] W. Van Schalkwijk and B. Scrosati, Boston, MA: *Springer*, 2002, 1 - 5 .

[35] Y. Chernyak, *J. Chem. Eng. Data,* 2006, **51**, 416 - 418.

[36] R. Payne and I.E. Theodorou, *J. Phys. Chem.,* 1972, **76**, 2892 - 2900.

[37] G. Kresse and J. Furthmüller, *Phys. Rev. B,* 1996, **54**, 11169.

[38] J.P. Perdew, K. Burke and M. Ernzerhof, *Phys. Rev. lett.,* 1996, **77**, 11169 - 11186.

[39] P.E. Blöchl, *Phys. Rev. B,* 1994, **50**, 17953 - 17979.

[40] G. Kresse and D. Joubert, *Phys. Rev. B,* 1999, **19**, 1758 - 1775.

[41] S. Grimme, S. Ehrlich and L. Goerigk, *J. Comput. Chem.,* 2011, **32**, 1456 - 1465.

[42] S. Grimme, J. Antony, S. Ehrlich and H. Krieg, *J. Chem. Phys.,* 2010, **132**, 154104.

[43] D. Santos-Carballal, A. Roldan, R. Grau-Crespo and N.H. de Leeuw, *PCCP,* 2014, **16**, 21082 - 21097.

[44] D. Santos-Carballal, A. Roldan and N.H. de Leeuw, *J. Phys. Chem. C,* 2016, **120**, 8616 - 8629.

[45] S.N.A. Zakaria, N. Hollingsworth, H. Islam, A. Roffey, D. Santos-Carballal, A. Roldan, W. Bras, G. Sankar, G. Hogarth, K.B. Holt and N.H. de Leeuw, *ACS Appl. Mater. Interfaces,* 2018, **10**, 32078 - 32085.

[46] D. Santos-Carballal, A. Roldan, N.Y. Dzade and N.H. de Leeuw, *Phil. Trans. Math. Phys. Eng. Sci.,* 2018, **376**, 20170065.

[47] S. Posada-Pérez, D. Santos-Carballal, U. Terranova, A. Roldan, F. Illas and N.H. de Leeuw N. H., *PCCP,* 2018, **20**, 20439 - 20446.

[48] V. Postica, A. Vahl, J. Strobel, D. Santos-Carballal, O. Lupan, A. Cadi-Essadek, N.H. de Leeuw, F. Schütt, O. Polonskyi, T. Strunskus, M. Baum, L. Kienle, R. Adelung and F. Faupel, *J. Mater. Chem. A,* 2018, **6**, 23669 - 23682.

[49] P.E. Blöchl, O. Jepsen and O.K. Andersen, *Phys. Rev. B,* 1994, **49**, 16223 - 16233.

[50] V.I. Anisimov, M.A. Korotin, J. Zaanen and O.K. Andersen, *Phys. Rev. lett.,* 1992, **68**, 345 - 348.

[51] D. Santos-Carballal, P.E. Ngoepe and N.H. de Leeuw, *Phys. Rev. B,* 2018, **97**, 085126.

[52] C.Y. Ouyang, S.Q. Shi and M.S. Lei, *J. Alloys Compd,* 2009, **474**, 370 - 374.

[53] J. Bhattacharya and C. Wolverton, *PCCP,* 2013, **15**, 6486 - 6498.

[54] A. Karim, S. Fosse and K.A. Persson, *Phys. Rev. B,* 2013, **87**, 075322.

[55] C.Y. Ouyang, X.M. Zeng, Z. Sljivancanin and A. Baldereschi, *J. Phys. Chem. C,* 2010, **114**, 4756 - 4759.

[56] R.J. Hill, J.R. Craig and G.V. Gibbs, *Phys. Chem. Miner.,* 1979, **4**, 317 - 339.

[57] D. Santos-Carballal, P.E. Ngoepe and N.H. de Leeuw, *Phys. Rev. B,* 2018, **97**, 085126.

[58] S. Chitra, P. Kalyani, T. Mohan, M. Massot, S. Ziolkiewicz, R. Gangandharan, M. Eddrief and C. Julien, *Ionics,* 1998, **4**, 8 - 15.

[59] P. Strobel, G. Rousse, A. Ibarra-Palos and C. Masquelier, *J. Solid State Chem.,* 2004, **177**, 1 - 5.

[60] M. Nakayama, H. Taki, T. Nakamura, S. Tokuda, R. Jalem and T. Kasuga, *J. Phys. Chem. C,* 2014, **118**, 27245 - 27251.

[61] S. Kim, M. Aykol and C. Wolverton, *Phys. Rev. B,* 2015, **92**, 115411.

[62] S. K. Mishra and G. Ceder, *Phys. Rev. B,* 1999, **59**, 6120 - 6130.

[63] P.W. Tasker, *J. Phys. C: Solid State Phys.,* 1979, **12**, 4977 - 4984.

[64] G. W. Watson, E. T. Kelsey, N. H. de Leeuw, D. J. Harris and S. C. Parker, *J. Chem. Soc. Faraday Trans.,* 1996, **92**, 433 - 438.

[65] R. Benedek and M.M. Thackeray, *Phys. Rev. B,* 2011, **83**, 195439.

[66] Y.K. Lee, J. Park and W. Lu, *J. Electrochem. Soc.,* 2016, **163**, A1359 - A1368.

[67] R.E. Warburton, H. Iddir, L.A. Curtiss and J. Greeley, *ACS Appl. Mater. Interfaces,* 2016, **8**, 11108 - 11121.

[68] D. Santos-Carballal, A. Roldan, R. Grau-Crespo and N.H. de Leeuw, *PCCP,* 2014, **16**, 21082 - 21097.

[69] C.M. Fang, S.C. Parker and G. de With, *J. Am. Ceram. Soc.,* 2000, **83**, 2082 - 2084.

[70] M. Masia, M. Probst and R. Rey, *J. Phys. Chem. B,* 2004, **108**, 2016 - 2027.

[71] Y. Wang, S. Nakamura, M. Ue and P.B. Balbuena, *J. Am. Chem. Soc.,* 2001, **123**, 11708 - 11718.

[72] L.B. Silva and L.C.G. Freitas, *J. Mol. Struct. Theochem,* 2007, **806**, 23 - 34.

[73] E.G. Leggesse, k.H. Tsau, Y.T. Liu, S. Nachimuthu and J.C. Jiang, *Electrochim. Acta,* 2016, **210**, 61 - 70.

[74] T. Takada, H. Hayakawa, H. Enoki, E. Akiba, H. Slegr, I. Davidson, J. Murray, *J. Power Sources,* 1999, **81 - 82**, 505 - 509.

[75] H. Huang, C.A. Vincent, P.G. Bruce, *J. Electrochem. Soc.,* 1999, **146**, 3649 - 3654.

[76] J.S. Kim, K. Kim, W. Cho, W. H. Shin, R. Kanno and J. W.Choi, *Nano lett.,* 2012, **12**, 6358 - 6365.

[77] S. Matsuyama, S. Kinugasa, K. Tanabe and T. Tamura, "Spectral Database for Organic Compounds, SDBS," National Institute of Advanced Industrial Science and Technology (AIST), 31 03 1999. [Online]. Available: https://sdbs.db.aist.go.jp/sdbs/cgi-bin/landingpage?sdbsno=2392. [Accessed 30 11 2018].

[78] B. Fortunato, P. Mirone and G. Fini, *Spectrochim. Acta A Mol. Biomol. Spectrosc.,* 1971, **27**, 1917 - 1927.

383

384